Qian, J., Meng, Q., Zhang, L., **Schlink, U.**, Hu, X., Gao, J. (2023):
Characteristics of anthropogenic heat with different modeling ideas and its driving effect on urban heat islands in seven typical Chinese cities
Sci. Total Environ. **886** , art. 163989

https://doi.org/10.1016/j.scitotenv.2023.163989

Dependence of urban heat islands on anthropogenic heat emissions: A synthesis from seven typical cities in China

Jiangkang Qian[a,b], *Qingyan Meng*[a,b,c,*], *Linlin Zhang*[a,b,c], *Uwe Schlink*[d], *Xinli Hu*[a,b,c],

Jianfeng Gao[a,b]

a. Aerospace Information Research Institute, Chinese Academy of Sciences, Beijing, 100094, China
b. University of Chinese Academy of Sciences, Beijing, 100049, China
c. Key Laboratory of Earth Observation of Hainan Province, Hainan Aerospace Information Research Institute, Sanya, 572029, China
d. Department of Urban and Environmental Sociology, Helmholtz Centre for Environmental Research-UFZ, Leipzig, D-04318, Germany
*Corresponding author: Qingyan Meng
E-mail addresses: mengqy@radi.ac.cn

Abstract

Anthropogenic heat (AH), an important urban heat source, is often overlooked or simplified in research on the driving mechanisms of the urban heat island effect (UHI), and case studies investigating the impacts of different AH estimation methods are scarce. This study estimated the AH in seven typical Chinese cities based on a remote sensing surface energy balance model ($\mathrm{AH_{seb}}$) and an energy consumption inventory-machine learning model ($\mathrm{AH_{inv}}$). The intensity of the surface UHI was extracted using land surface temperatures, and then the linear mixed-effects model and geographic detectors were used to analyze the driving effect of AH on the UHI. Despite the similar shapes of the spatial profile curves, the AH derived from the two models differed in both temporal and spatial characteristics, which was more typical in winter and in urban centers, and $\mathrm{AH_{inv}}$ had a more notable central spread feature than $\mathrm{AH_{seb}}$. The AH driving effects on UHI were notably influenced by spatial and temporal heterogeneity, particularly in regions with distinct background climates. However, after controlling for the random effects of the background climate, AH still exhibited a considerable enhancing effect on the UHI. AH_{seb} outperformed AH_{inv} in terms of linear positive correlation and interpretation rate for UHI. Meanwhile, interactions with other potential factors enhanced AH driving effects. This study offers guidance for simulating and analyzing urban climates to propose practical and effective measures for optimizing urban thermal environments, with a focus on AH or and energy consumption control.

Key words: Anthropogenic heat, Urban heat islands, Driving analysis, Spatiotemporal heterogeneity

1. Introduction

Urbanization has had the greatest impact on the transformation of the Earth's environment, as evidenced by the growth in urban area and population in recent decades (Chapman et al., 2017; Zhou et al., 2018). During the rapid process of urbanization, natural landscapes are replaced with impervious surfaces, changing the properties and geometries of the ground surface and influencing energy absorption, storage, and emission, as well as releasing additional anthropogenic heat (Firozjaei et al., 2020; Meng et al., 2018; Mirzaei and Haghighat, 2010; Voogt and Oke, 2003). Urban heat islands (UHIs) are a major environmental issue caused by urbanization, with substantially impacts on urban climate, ecology, and human health (Mohajerani et al., 2017; Ulpiani, 2021; Yang et al., 2022b). Understanding the underlying mechanisms of UHI is crucial for developing effective measures to optimize the quality of human living space (Meng et al., 2022).

Land surface temperature (LST) obtained through thermal infrared remote sensing has broader applicability compared to site-based atmospheric temperature measurements, which have spatial limitations (Bahi et al., 2019; Dewan et al., 2021). LST can determine the spatial and temporal characteristics of UHI and enhance our understanding of urban climate dynamics (Hu et al., 2020; Ward et al., 2016; Wu et al., 2022). Therefore, surface UHI based on LST has become a crucial aspect in urban thermal environment studies (Fu et al., 2022; Peng et al., 2012). The formation of UHIs is a result of a complex interaction between multiple factors affecting surface energy balance (Rizwan et al., 2008; Zhao et al., 2014); in recent years, there has been extensive exploration of the patterns driving UHIs in multiple regions and time periods. To identify feasible measures for thermal environment mitigation under specific climatic and geographic conditions, a wide range of potential UHI drivers related to urbanization are considered using statistical or machine learning methods. These drivers include factors such as vegetation and water distribution, the characteristics of artificial surfaces, landscape patterns, three-dimensional building structures, and human activity (Dewan et al., 2021; Fu et al., 2022; Hu et al., 2020; Hu et al., 2022; Liang et al., 2020; Meng et al., 2022; Mohajerani et al., 2017; Ramirez-Aguilar and Lucas Souza, 2019; Wang et al., 2021b). However, most current studies focus on the difference in energy balance between urban and rural areas due to changes in the physical properties of the land surface resulting from urbanization, often overlooking or simplifying anthropogenic heat (AH), which is a key energy source and driver of the urban thermal environment (Chapman et al., 2017; Peng et al., 2012; Yang et al., 2022a). Instead, socioeconomic variables such as nighttime lighting, population density, gross domestic product, and road networks have been used as proxies for AH in UHI studies (Liang et al., 2020; Raj et al., 2020; Wang et al., 2021b; Wang et al., 2021c; Zhou et al., 2014), although these factors are not directly correlated with LST. The difficulties in obtaining AH data with spatial and temporal heterogeneity may be an important impediment to relevant studies (Dong et al., 2017; Sun et al., 2018).

To support the exploration of the impact of AH on the urban thermal environment, numerous implementable AH estimation methods, models, and datasets have been proposed. These can be divided into three categories: energy consumption inventory methods, surface energy balance methods, and building energy simulation methods (Sailor, 2011). Building energy simulation is considered the most accurate method for determining building heat emissions, but it has a high demand for data and cannot be applied in large-scale studies (Alhazmi et al., 2022; Nie et al., 2014; Vahmani et al., 2022). The energy consumption inventory method is the most common method for estimating AH and is highly applicable and scalable in various studies (Quah and Roth, 2012; Smith et al., 2009; Varquez et al., 2021). With advancements in communication and network technologies, big data with location-based semantic information, spatial interaction information, and real-time dynamic information have great potential in representing and explaining the spatiotemporal characteristics of human activities (Chen et al., 2020; Gao et al., 2017); combining these data with inventory methods can effectively improve the resolution of AH estimation (Liu et al., 2021; Ming et al., 2022; Xu et al., 2021). Furthermore, the combination of machine-learning algorithms allows for more accurate and applicable AH models (Chen et al., 2020; Qian et al., 2022; Wang et al., 2022b). The surface energy balance (SEB) method uses micro-meteorological observation techniques such as the eddy covariance system to determine the terms in the SEB equation, with the residual term considered as the AH (Pigeon et al., 2007). The combination of SEB with quantitative remote sensing techniques (RS-SEB) allows for application on larger spatial scales (Kato and Yamaguchi, 2005), making it one of the most effective methods for obtaining high-resolution AH and a common means of validating the results of AH estimation (Chow et al., 2014; Peng et al., 2021; Zhou et al., 2012). Due to the strengths and weaknesses of various methods, multi-method mixed modeling and cross-validation have become an important direction for future AH studies (Wang et al., 2022a; Zheng and Weng, 2018). However, further investigation is necessary to examine the differences in the spatial and temporal distribution of AH estimated by different methods and its impact on the urban thermal environment.

The study of the impact of AH on the urban thermal environment is still in the early stages of numerical simulation experiments (Molnar et al., 2020; Singh et al., 2022; Tao et al., 2022; Zhan and Xie, 2022) and lacks systematic analysis in real cases. Based on refined AH data, the role of AH in the urban thermal environment can be reflected more intuitively and convincingly through a mature statistical-based analysis from UHI driving studies (Hu et al., 2020), which also provide example arguments for numerical simulation studies. In this study, AH was modeled in seven cities in different geographic regions of China using two methods. The objectives of this study were to 1) investigate the differences in the spatial and temporal characteristics of different AH results, 2) explore the important relationships between AH and

UHI, and 3) examine the impacts of AH on UHI and its interactions with other potential factors.

2. Study area and dataset

2.1. Study area

Since the late 1970s, China has undergone unprecedented economic development and urbanization (Cao et al., 2016; Schneider and Mertes, 2014; Yang et al., 2019), resulting in a dramatic increase in energy consumption and associated AH emissions. This has altered the energy flow in urban ecosystems and affected urban ecological processes such as urban regional climate and atmospheric environment, causing frequent extreme heat events, decreased air quality, and serious impacts on the health of residents in Chinese cities (Cong et al., 2022; Gu et al., 2016). One representative central city from each of the seven natural geographic regions of China (Zhao et al., 2015) was selected as the target area (**Fig. 1**). These cities serve as the economic, cultural, and transportation hubs of their respective regions and as well as the entire country, and they exhibit considerable variations in climate, topography, and other natural conditions. Hence, studying the driving mechanisms of AH and UHI in these cities will provide valuable information for urban thermal environment management. Due to their close integration, Foshan and Guangzhou are treated as one region in this study and are referred to as Guangzhou in the following text.

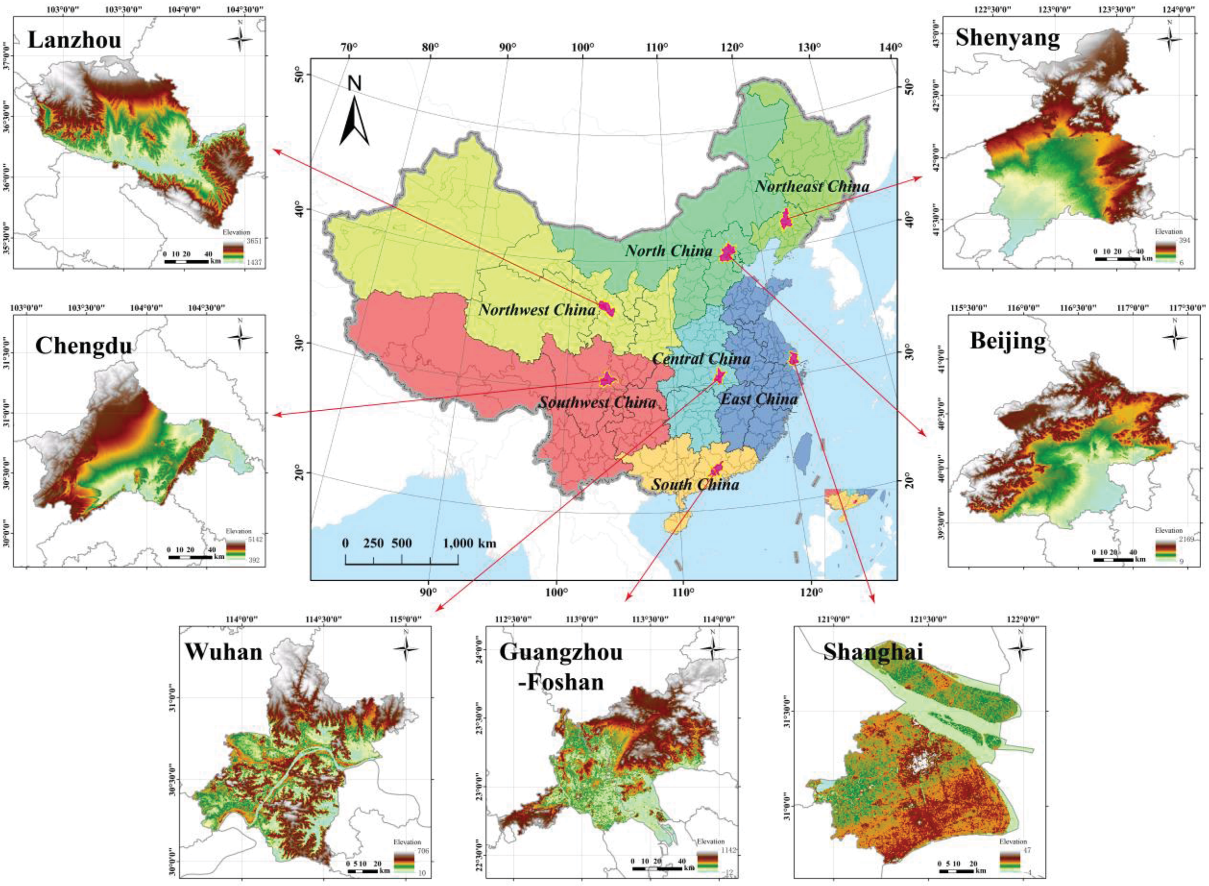

Fig. 1. Geographical location, terrain, and administrative extents of the study areas.

2.2. Dataset

To calculate UHI intensities and obtain the surface parameters required for the RS-SEB model, the following data were used: MOD11A1 1000m resolution daily surface temperature and emissivity product, MOD09GA 500m resolution daily surface reflectance product from NASA (https://ladsweb.nascom.nasa.gov), ALOS 30m resolution global digital surface model (DSM) dataset (Tadono et al., 2016), 2017 10m resolution global land cover data, and 30m resolution global artificial impervious surface data (Gong et al., 2020; Gong et al., 2019). The meteorological parameters required for the RS-SEB model were obtained from the National Centers for Environmental Information site data (NCEI GIS Team, 2021) and ERA5 atmospheric reanalysis data (Muñoz Sabater, 2019) corresponding to the Terra satellite crossing moment.

The energy consumption inventory-machine learning model used in this study is based on a previous study (Qian et al., 2022) and requires a large and diverse dataset including energy consumption, socioeconomic, point-of-interest, road/railway, nighttime illumination, surface temperature, and meteorological, and topographical data. The data sources and preprocessing are described in the original study (Qian et al., 2022). Additionally, population heat data obtained from cell phone user location information from the Baidu Huiyan big data platform (https://huiyan.baidu.com) were also included in this study to describe the dynamic population aggregation within the city to estimate the hourly gridded AH. The monthly average data for July and December 2017 (2016 for Guangzhou) in the study area were obtained based on the above data sources.

3. Method

This study was divided into two major parts (**Fig. 2a**): AH estimation and UHI driving analysis of the mean satellite transit moment in summer (July) and winter (December). First, the AH was estimated using a machine learning model that combined the energy inventory method and a remote sensing surface energy balance model. After the UHI intensity was calculated, a linear mixed-effects model and geographic detectors were used to examine the important relationships between AH and UHI.

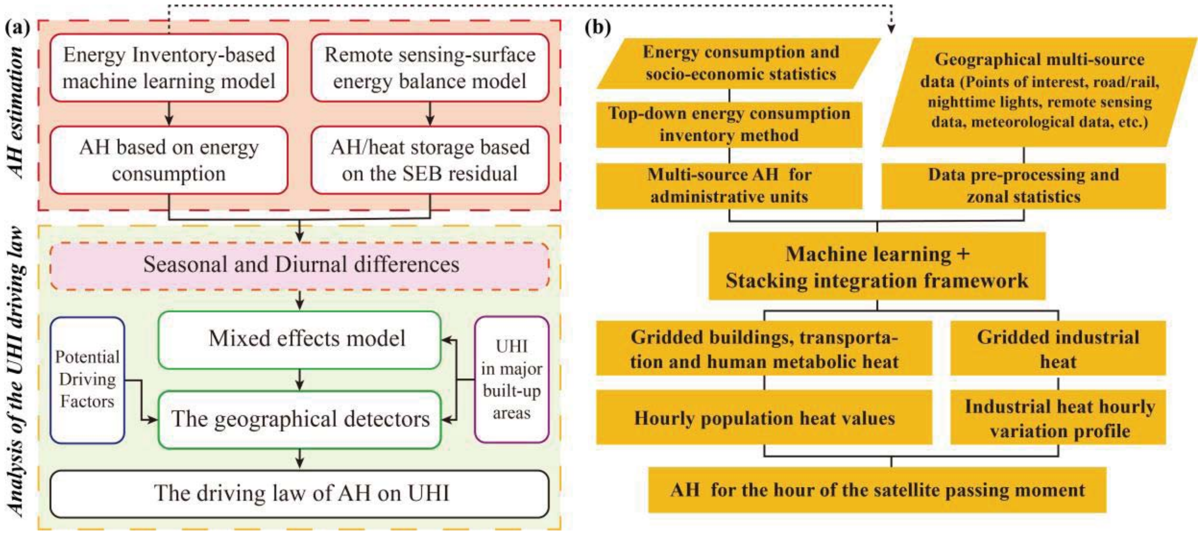

Fig. 2. Workflow for (a) the whole study and (b) the energy inventory-machine learning model. AH: anthropogenic heat, SEB: surface energy balance, UHI: urban heat island.

3.1 AH estimation

3.1.1. Inventory based-machine learning method

The most common AH estimation method is the top-down energy consumption inventory method, which is based on large-scale energy consumption data and is downscaled step-by-step using specified spatial-temporal rules. In our previous study (Qian et al., 2022), we constructed an efficient AH estimation model combined with top-down inventory and machine learning (ML) algorithms. Further details on the data preprocessing, AH sample estimation, and model training evaluation can be found in Qian et al. (2022). Therefore, this study improved the training process of ML models using the stacking integration framework (Wolpert, 1992) to fully exploit the advantages of various ML algorithms. Furthermore, the monthly AH from the ML model is the average of the whole-day AH for that month, which may be further refined in time scales to obtain the AH at the Terra satellite transit moment for that month (**Fig. 2b**). The intraday variations in multi-source AH were estimated using population heat (PH) data within each grid and the intraday variation curve of industrial heat proposed in previous studies (Liu et al., 2021; Zheng and Weng, 2018). The AH obtained using this method is denoted as $\mathrm{AH_{inv}}$ and is calculated as follows:

$$AH_{inv}^{h} = f_{h1} \cdot AH_{1}^{m} + f_{h2} \cdot AH_{2}^{m} \tag{1.}$$

$$f_{h2} = \frac{d_1 \times ph_{h1} + d_2 \times ph_{h2}}{d_1 \times ph_{d1} + d_2 \times ph_{d2}} \tag{2.}$$

where AH_{inv}^{h} denotes the mean AH ($W \cdot m^2$) at time h of satellite transit for the corresponding month, AH_{1}^{m} is the monthly mean industrial heat from the ML model, f_{h1} is the intraday variation coefficient of industrial heat (%), AH_{2}^{m} is the monthly mean transportation heat, building heat, and metabolic heat from the ML model, and f_{h2} is the intraday variation coefficient of population (%). ph_{h1} and ph_{h2} are the PH values at time h in that month for weekdays and weekends, d_1 and d_2 are the number of weekdays and weekends in that month, and ph_{d1} and ph_{d2} are the average PH values for the entire day on weekdays and weekends. Detailed information about the stacking framework is provided in the **Appendix**. For the sake of brevity, AH derived using this method is hereafter referred to as $\mathrm{AH_{inv}}$. Both the calculation process and results have a resolution of 500 m.

3.1.2. Remote sensing-surface energy balance model

AH has been recognized as an important source term in urban multiscale energy systems (Chapman et al., 2017; Pigeon et al., 2007), whereas the sum of the energy received and released from the surface system remains constant during transformation and transfer, and the surface energy balance method considers the residual term of the energy budget as the AH-induced disturbance. Kato and Yamaguchi (2005) first proposed the remote sensing surface energy balance (RS-SEB) model for AH estimation. This model, which applies quantitative remote sensing techniques to estimate surface energy, has been widely adopted in urban-scale studies (Firozjaei et al., 2020; Wong et al., 2015; Yu et al., 2021). In this study, a similar RS-SEB model was constructed to estimate the daytime AH following the previous modeling process:

$$AH = R_n - (H + LE + G) \tag{3.}$$

where R_n denotes the net radiation, H represents the sensible heat flux, LE is the latent heat flux, and G indicates ground or conductive heat flux at the material surface. However, due to the uncertainty in the calculation of parameters at night, G and AH are combined as the principal surface heat sources during nighttime to represent the release of heat storage at night (Kato and Yamaguchi, 2007):

$$\Delta S = AH - G = H + LE - R_n \tag{4.}$$

where ΔS represents the intensity of heat storage release at night and its magnitude reflects the intensity of AH at the city scale. Considering the coarse spatial resolution of thermal infrared remote sensing, the influence of mixed pixels on the calculation of surface parameters required for RS-SEB cannot be overlooked (Liu et al., 2020). Therefore, in this study, fixed surface parameters such as aerodynamic resistance were computed using high-resolution DSM and land cover data, and their pixel values at coarse resolution (500 m) were calculated using sub-pixel aggregation. For specific information on RS-SEB parameter calculation and model construction, please refer to Kato and Yamaguchi (2005) and Zhou et al. (2012). For brevity, the AH with a spatial resolution of 500 m based on this method is referred to as $\mathrm{AH_{seb}}$.

3.2. UHI intensity

In this study, urban heat island intensity (UHII) was defined as the difference between the urban LST and the mean LST of the surrounding rural areas (Clinton and Gong, 2013; Zhou et al., 2014), Therefore, the boundaries of the urban built-up areas and rural areas of the city must be determined. The impervious surface distribution density (ISDD) was calculated to describe the extent and density of impervious surface in a specified radius around a pixel (Firozjaei et al., 2020; Meng et al., 2018):

$$ISDD_s(r) = \frac{\sum_{i=1}^{n} B_{si} \cdot \left(1 - \frac{D_i}{2r}\right)}{\sum_{i=1}^{n} \left(1 - \frac{D_i}{2r}\right)} \tag{5.}$$

where *s* represents the center pixel, B_{si} is the value of the *i*th pixel within radius *r* (impervious pixel = 1; permeable pixel = 0), D_i is the distance between pixel *i* and the center pixel, and *n* is the total number of pixels within a circle of radius *r* (1,000 m). Urban built-up area boundaries were extracted using the city clustering algorithm (CCA) based on the obtained ISDD (Rozenfeld et al., 2008). The rural area in this study is defined as a buffer zone around an urban area that is the same size as the urban area (Dewan et al., 2021; Zhou et al., 2014); the UHII can be calculated using the following equation:

$$UHII = LST_u - \overline{LST_r} \tag{6.}$$

where LST_u represents the surface temperature within the urban area of the city and $\overline{LST_r}$ is the average surface temperature in rural areas.

3.3. Relationship between AH and UHI

Linear mixed-effects models and geographic detectors were used to elucidate the relationship between AH and UHI. AH estimation models are the empirical and physical expressions of this intrinsic relationship; however mathematical and statistical approaches can provide a more intuitive and interpretable result.

3.3.1. Mixed effects model

This study aimed to determine the practical contribution of AH to UHII by using a linear mixed-effects model. In multi-regional and multi-temporal studies, UHII is largely determined by climatic context, including geographical area, season, and diurnal factors. Thus, the role of AH may not be significant. Mixed-effects models (Bollen and Brand, 2010; Sheiner and Grasela, 1991) could be used to address this issue. We treated the variation in UHII with AH as a fixed effect, while regional, seasonal, and diurnal factors were considered random effects and were included in the analysis as categorical variables (**Table A1**). By excluding the random effects, we could determine the actual impact of AH in a multi-spatial and temporal environment, and also reflect the important role of climate context. In this study, nested effects between different random effects were considered and implemented in R, and the optimal mixed-effects model was selected based on the Akaike information criterion.

3.3.2. Geographic detectors

Geographic detectors are a set of statistical methods for detecting spatial differentiation and revealing the driving forces behind it. They are divided into four modules: factor detection, interaction detection, risk detection, and ecological detection (Wang and Hu, 2012; Wang et al., 2010). The basic assumption is that if an independent variable has a substantial effect on a dependent variable, the spatial distributions of the independent and dependent variables should be similar. Geographic detectors can identify complex linear and nonlinear relationships between independent and dependent variables, and the analysis results are not affected by multivariate covariance (Wang et al., 2021a). This study employed the factor detection module to measure the UHI spatial heterogeneity induced by AH, which is quantitatively described by the q-statistic:

$$q = 1 - \frac{\sum_{h=1}^{L} N_h \sigma_h^2}{N\sigma^2} \qquad (7.)$$

where h is the layering of the dependent variable Y or factor X, namely the classification or zoning, σ_h^2 and σ^2 are the variances of the Y values for layer h and the entire region, respectively. The value range of q is [0,1], and a larger value indicates a more notable spatial heterogeneity of Y or a stronger interpretation of Y by X. Interaction detection assesses the interaction of the two factors on the target variable, represented by the stacked q-value. In addition to AH, this study calculated UHI drivers that were commonly used in previous studies (Peng et al., 2012; Wu et al., 2022; Yang et al., 2017) to determine the interaction between AH and other drivers (**Table A2**), including landscape pattern index, class level index of impervious surface and vegetation, enhanced vegetation index (EVI) and surface albedo.

4. Results

4.1. Characteristics of AH distribution

The AH and nighttime ΔS values were obtained for the seven cities during spring and summer using both models (**Fig. 3**). The $\mathrm{AH_{inv}}$ was notably stronger during the day than at night in the same season, and it was stronger in summer than in winter in the southern regions (Shanghai, Wuhan, Chengdu, and Guangzhou), where summer temperatures were high and winter temperatures were relatively mild, but in the northern regions (Beijing, Shenyang, and Lanzhou), where winters are extremely cold, the winter $\mathrm{AH_{inv}}$ was stronger. For daytime

AH_{seb}, the AH values in the urban built-up area were much larger in summer than in winter, while the spatial distribution of ΔS at night in winter was more consistent with the urban boundaries. Despite the similar distribution ranges, the AH obtained by the two models differed in both temporal and spatial details. The extent and intensity of AH_{seb} were stronger than AH_{inv} in the summer in some cities, whereas AH_{seb} was generally weaker in the winter. The high values of AH_{inv} were remarkably clustered in the urban center and radiated outward, whereas the high values of AH_{seb} were mainly distributed in the low-rise areas and industrial areas around the urban areas, and were weak in the urban center with dense high-rise buildings.

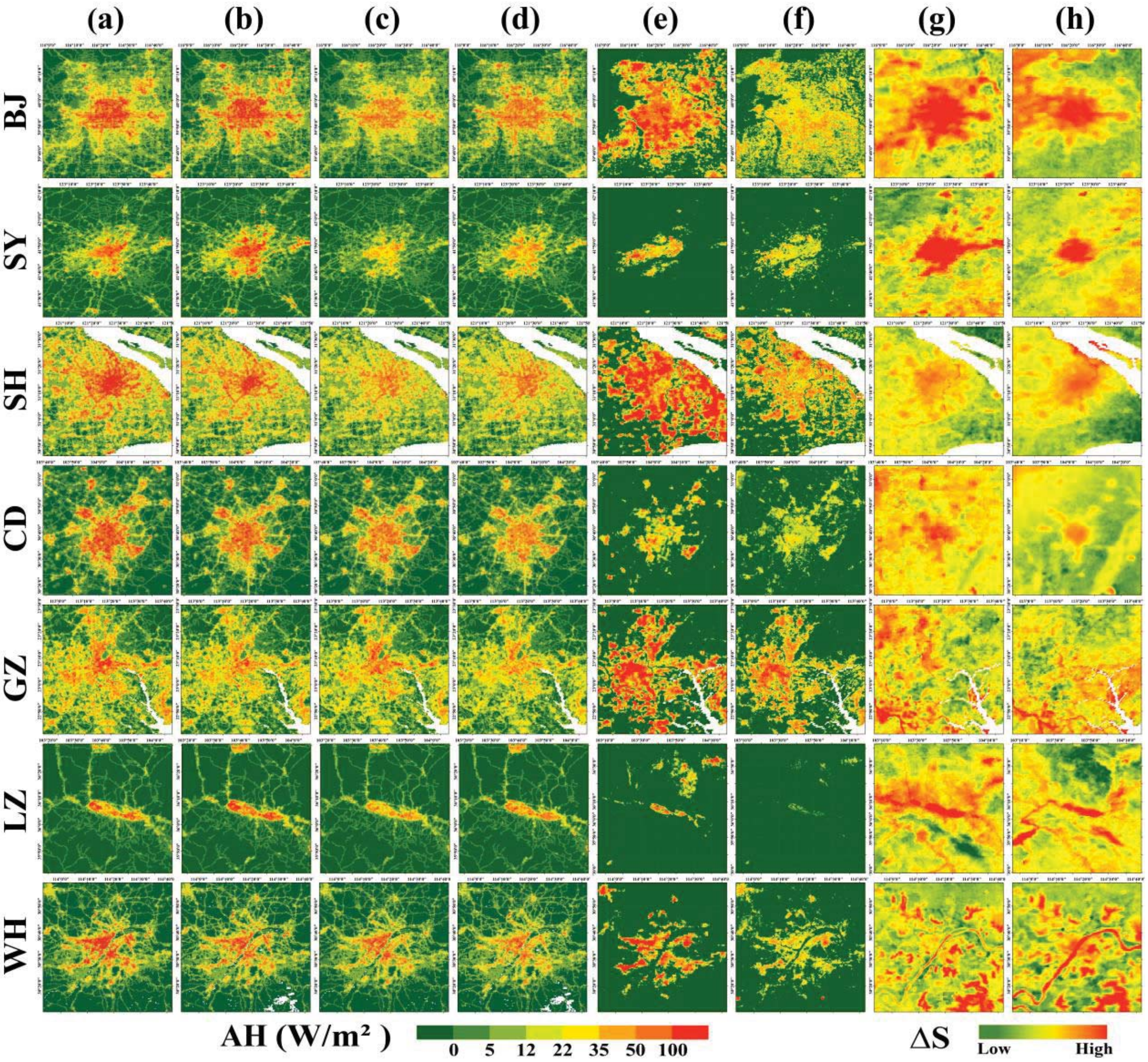

Fig. 3. Spatial and temporal distribution of anthropogenic heat and nighttime heat storage: (a)–

(d) $\mathrm{AH_{inv}}$ in summer daytime, winter daytime, summer nighttime and winter nighttime, respectively; (e)–(f) $\mathrm{AH_{seb}}$ in summer and winter daytime, respectively; (g)–(h) heat storage (ΔS) in summer and winter nighttime based on RS-SEB, respectively.

To better reflect the spatial and temporal differences in the results of the different models, the AH in Beijing and Shanghai were selected for the spatial profile visualization of urban areas (**Fig. 4**). AH exhibited a roughly peaked curve, with high values in the central region where the impervious aggregation density was the strongest. The summer daytime curves of AH for the two models were similar, particularly in regions dominated by built-up areas, whereas there were large differences in peripheral regions dominated by rural areas, primarily in the anomalously low and high values of $\mathrm{AH_{seb}}$ in the periphery regions. During the winter, $\mathrm{AH_{seb}}$ was lower than $\mathrm{AH_{inv}}$ during the daytime, especially in metropolitan areas. The $\mathrm{AH_{inv}}$ in Beijing was slightly lower at night than during the day, whereas the $\mathrm{AH_{inv}}$ in Shanghai decreased more notably at night. In contrast, the nighttime ΔS in Beijing was very strong, whereas the nighttime ΔS in Shanghai was closer to the daytime AH values. The spatial distribution of ΔS was smoother than that of the AH profiles.

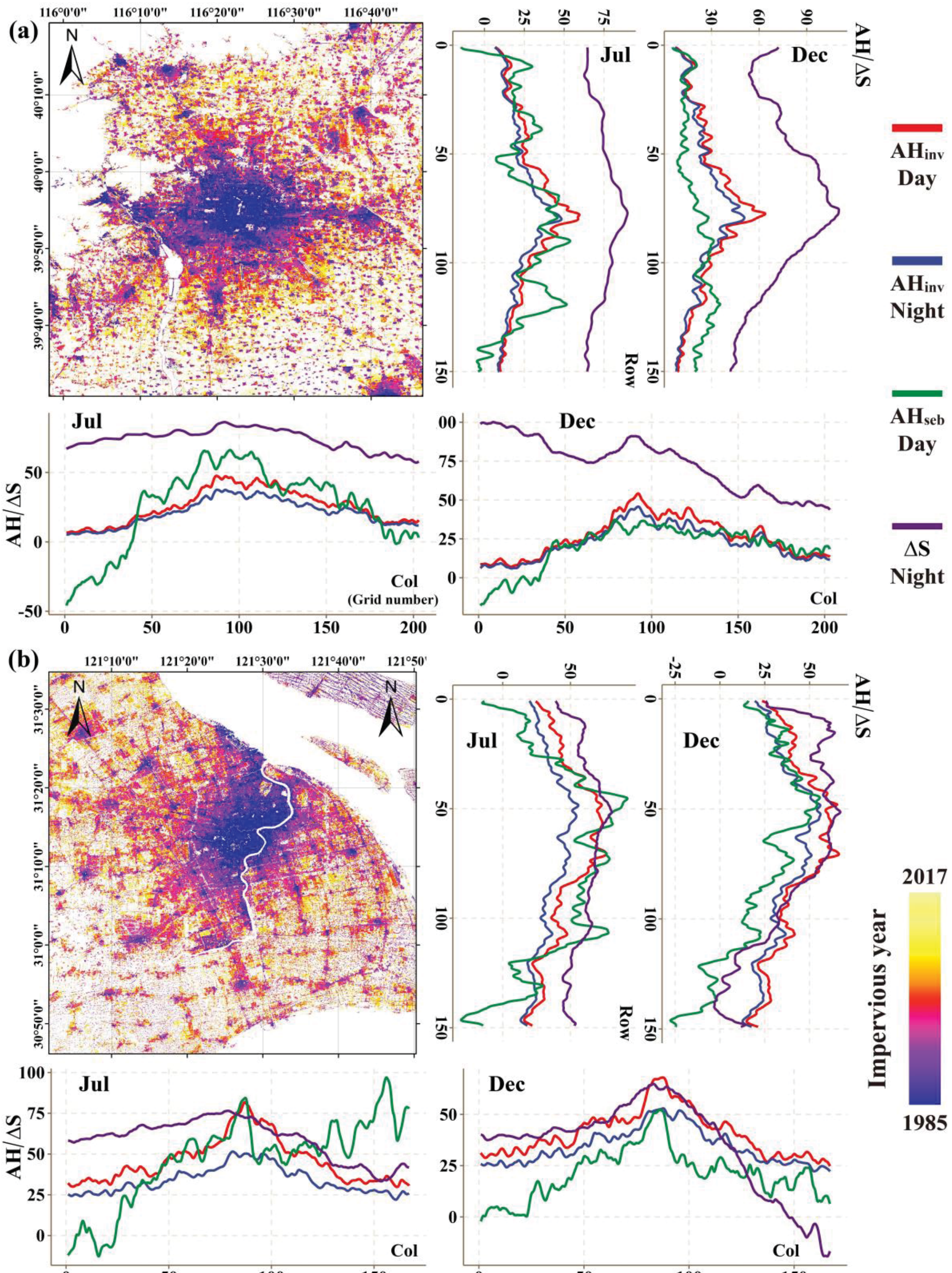

Fig. 4. Spatial profiles of AH and nighttime heat storage (ΔS) based on different methods in (a) Beijing and (b) Shanghai. Each unit of "Row" and "Col" refers to one grid (500 m) of rows and columns, respectively.

4.2. Relationship between AH and UHI

The spatial and temporal characteristics of UHI were determined using the LST map (**Fig.**

5 and **Table A3**). UHI was strongest during summer daytime in most regions, with the exception of Lanzhou, where an urban cold island was observed during the daytime in both summer and winter due to its arid and sparsely vegetated conditions. UHI was weaker during winter daytime compared to summer, but in Guangzhou, which is located in the tropics, the UHI was much stronger during winter daytime than in other regions, although the nighttime UHI was not pronounced. However, in most regions, a strong UHI was observed during both summer and winter nighttime, with a distinct central radiative distribution.

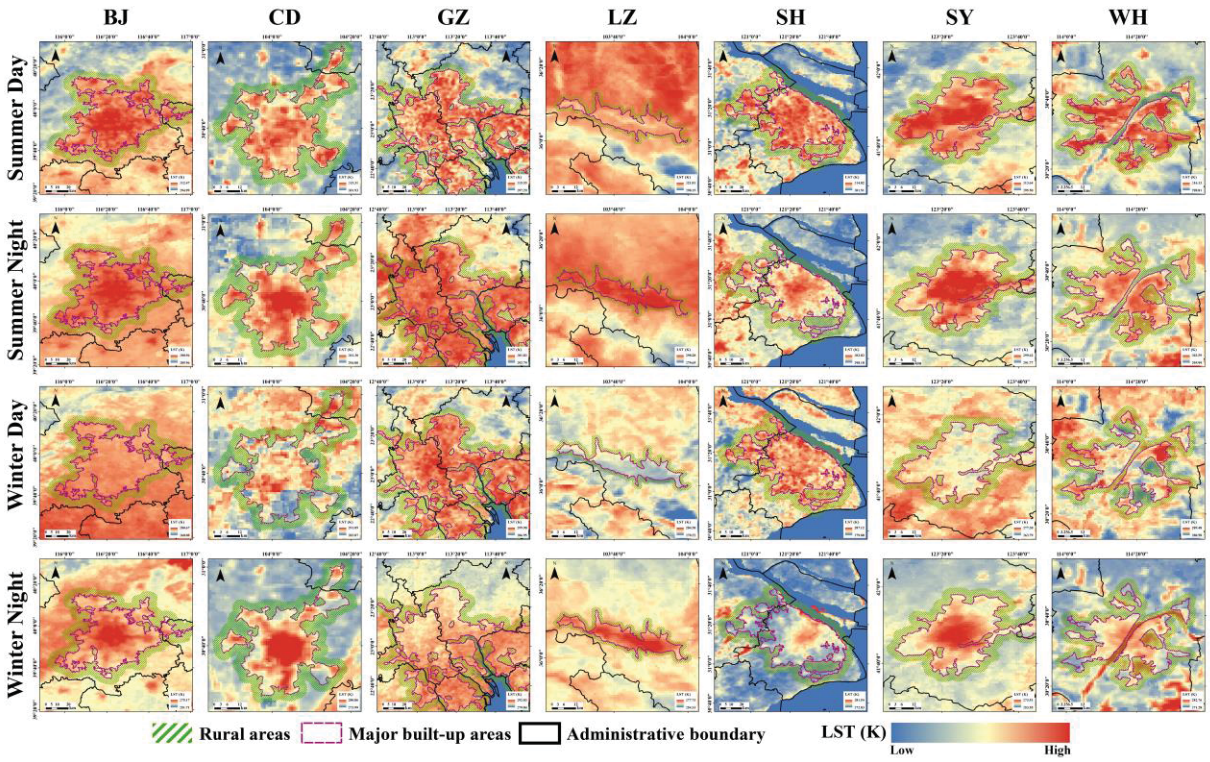

Fig. 5. Surface temperatures in major built-up and rural areas in each city at different time periods.

In general, there was a clear positive relationship between the AH and UHII (**Fig. 6**). The positive relationship between AH_{inv} and UHII was strong during summer daytime in most cities, but weak during the winter daytime and relatively substantial at night. However, the relationship between AH_{inv} and UHII in Lanzhou and Guangzhou was different: notable in

Lanzhou only at night and in Guangzhou only during the daytime. Compared with $\mathrm{AH_{inv}}$, $\mathrm{AH_{seb}}$ and nighttime ΔS had stronger linear correlations with UHII, and this relationship was highly significant (p<0.001) in most cases. The results of the mixed-effects model (**Table 1**) indicated that random effects, such as regional, seasonal, and diurnal effects, had high variance, suggesting a substantial impact on the UHI. After excluding random effects, the positive linear contribution of AH to UHI remained significant (p<0.001). This shows the fixed warming effect of AH in the urban thermal environment, and the slope is a measure of the impact of AH on UHII. The greater slope of $\mathrm{AH_{seb}}$ indicated a stronger influence than $\mathrm{AH_{inv}}$, but the larger random effects also implied that AH_{seb} was more susceptible to interference from the urban background climate.

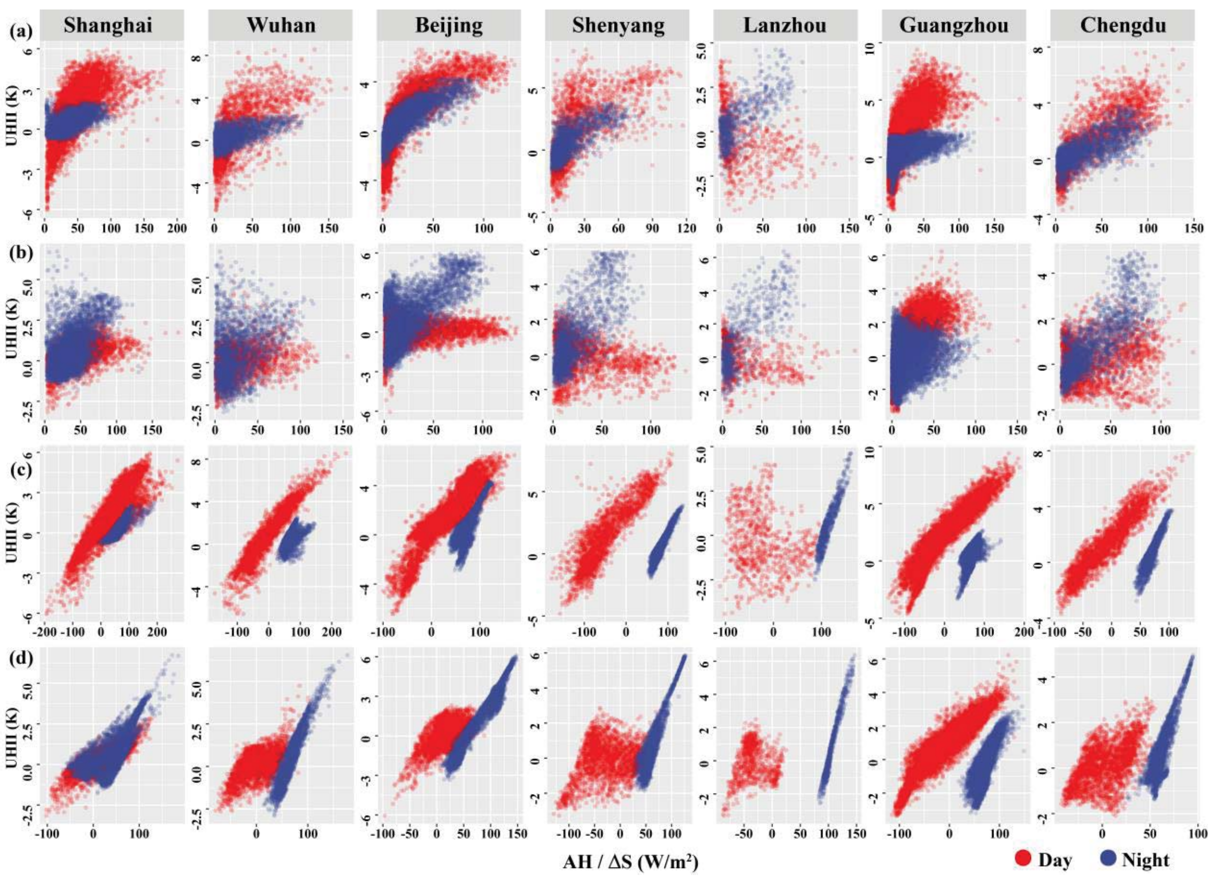

Fig. 6. Relationship between UHII and (a)–(b) $\mathrm{AH_{inv}}$ for summer and winter, respectively; (c)–(d) daytime $\mathrm{AH_{seb}}$ and nighttime ΔS for summer and winter, respectively, in major built-

up and rural areas.

Table 1. Results of the mixed-effects model based on AH and UHII (Z-Score normalization).

AH type	Random effect		Fixed effect	
	Random term	Variance explanation	Intercept	Slope
AH_{inv}	AH | Region/Season/Time	39 %	-0.02	0.49***
AH_{seb}	AH | Region/Season	74 %	-0.04	0.66***

4.3. The driving effects of AH on UHI

The q-value of the geographic detectors captured the extent to which the independent variables accounted for the target variables and explored the role of AH in driving surface UHI (**Fig. 7**). The interpretation rate for AH_{inv} was higher during summer and winter nights. In all cities except Guangzhou and Lanzhou, the interpretation rate of AH_{inv} was not greatly different between summer daytime and nighttime. The interpretation rate of AH_{inv} was much stronger during winter nighttime than daytime in most cities, but the opposite was true for Guangzhou. The explanatory rate of daytime AH_{seb} was generally higher than that of AH_{inv} and was stronger in summer than in winter. The explanatory rate of nighttime ΔS was the strongest for UHI, particularly during winter nighttime. However, the interpretation rate of nighttime ΔS in Guangzhou was lower than that of AH_{seb} in daytime for both winter and summer. Overall, the results from the different AH models showed notable differences in terms of the driving effects on UHI in multiple spatial and temporal scenarios.

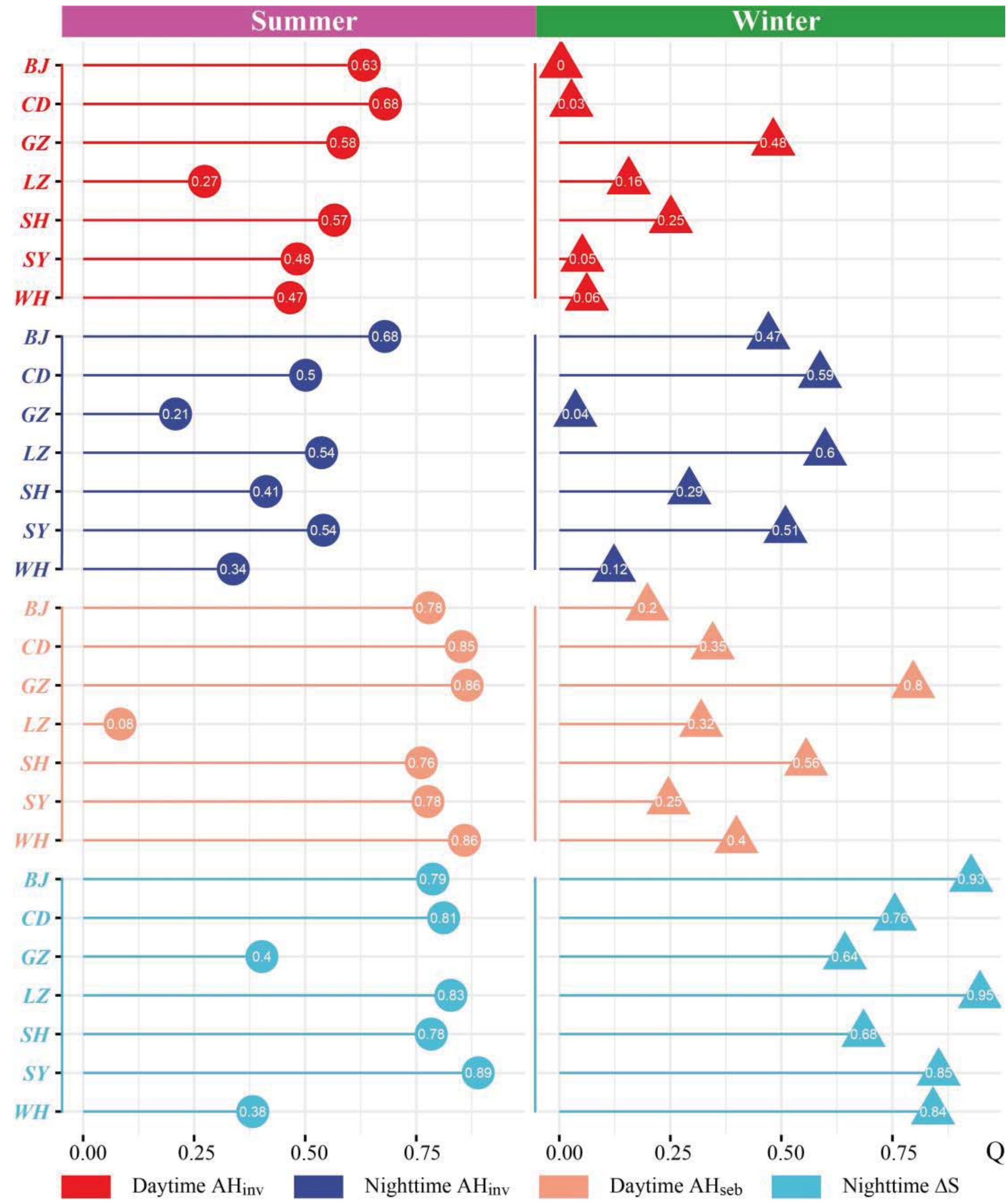

Fig. 7. Interpretation rate (q-value) of AH and ΔS on UHII calculated using factor detection.

The interaction between AH and all the factors improved the interpretation rate for UHI (**Fig. 8**). Generally, the interactions were similar to the results of the separate effects of AH, with the interaction of AH having the lowest interpretation rate during winter daytime and a relatively high rate during summer daytime, except for Guangzhou and Lanzhou. The effects of these factors did not differ greatly, but were influenced by spatial and temporal heterogeneity. For the interaction of AH_{inv}, the impervious surface and vegetation factors differed considerably, particularly at night with clear dividing lines in the interpretation rate plot, whereas albedo was a more prominent factor, often exhibiting large differences from the other factors and was the most dominant enhancer during winter daytime when the overall interpretation was low. The interaction characteristics of the other factors with AH_{seb} and ΔS were similar to AH_{inv}, but the interaction was stronger due to the higher explanatory rate of AH_{seb} and ΔS, which could even reach 100% in Beijing and Lanzhou during winter nights. The role of albedo, however, was not as prominent in AH_{seb} and ΔS and the interaction interpretation rate of the landscape-level factors was weak.

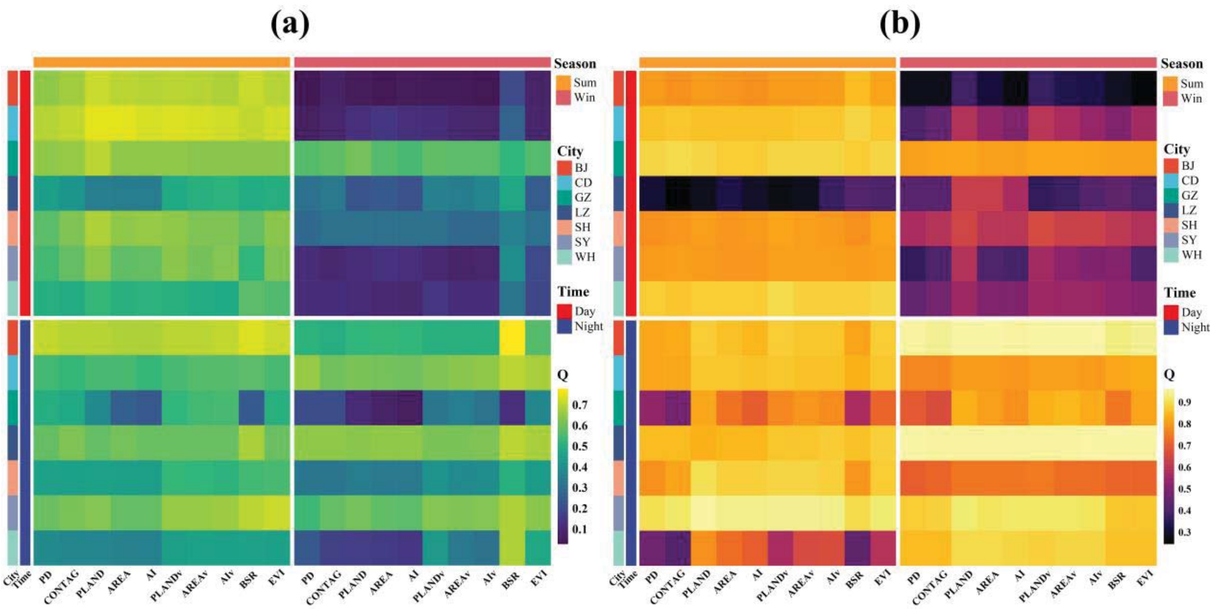

Fig. 8. Interaction interpretation rate for UHII (q-value) between other driving factors and (a) AH_{inv}, (b) AH_{seb} and nighttime ΔS.

5. Discussion

5.1. Implications of the AH from different methods

The distinction between the inventory-based method and the energy balance method was evident in the definition and calculation of AH, which was reflected in the spatial and temporal distribution of AH and its relationship with UHI. The method based on energy consumption inventories follows the assumption that heat generated from anthropogenic energy consumption is immediately released into the atmosphere as sensible heat (Kotthaus and Grimmond, 2012; Smith et al., 2009). However, in reality, this heat is absorbed, stored, or dissipated into the atmosphere as latent heat. Thus, AH_{inv} should be considered as the maximum sensible heat generated by anthropogenic activities. In contrast, RS-SEB ignores the perturbation of AH on terms other than the sensible heat term; thus, AH_{seb} could be considered as an increase in near-surface atmospheric sensible heat caused by AH (Firozjaei et al., 2020; Kato and Yamaguchi, 2005). This explains why AH_{seb} had a stronger linear correlation and explanatory rate with the surface UHI. In urban centers with a high density of high-rise buildings, AH_{seb} was generally lower than AH_{inv} due to non-negligible heat storage perturbation and impacts of building shading, and stronger heat storage efficiency in winter further reduced its value (Kato and Yamaguchi, 2007; Wong et al., 2015; Yu et al., 2021). Because AH_{inv} is derived from urban energy consumption and does not have a direct effect on the urban thermal environment, its interpretation of UHI was lower. However, its interaction with other factors could be explained as the efficiency of AH_{inv} as sensible heat release, causing an increase in LST. The interaction of AH_{seb} with other factors represents the warming effect of anthropogenic sensible heat influenced by surface properties and is influenced by the urban background climate, building materials, and meteorological conditions. At night, the main energy source besides AH is the heat stored in urban surface materials that dissipates in the form of long-wave radiation (Zheng et al., 2021; Zhou et al., 2014). Therefore, the ΔS in this study reflected the

UHI distribution at night and confirmed the determining effect of the combined contribution of artificial surfaces and AH sources to the nighttime UHI.

In general, the differences in physical meanings and numerical values determine the differences in the distribution characteristics and environmental effects of AH_{inv} and AH_{seb} under various conditions. When examining the characteristics of human activities and their environmental impact, AH_{inv} is more appropriate, as it comes directly from energy consumption and social economy, whereas AH_{seb} is a better choice for urban energy budgets and direct impacts on the thermal environment. However, the suitability of these methods is not absolute as the definitions of the AH input required by analytical or simulation methods must be considered. Clarifying the implications of AH input is critical to obtain more accurate and robust conclusions when investigating the driving role of human activities on UHI.

5.2. Implications for UHI mitigation

The inclusion of AH in climate simulations can considerably improve model performance and reliability for meteorological parameters and air pollutants, whereas urban numerical simulation studies that do not consider AH are physically incomplete (Chen et al., 2016; Molnar et al., 2020). Because of the differences in the implications of AH estimated via different methods, there are limitations in using only a broad definition of AH to study the urban thermal environment and climate change (Liu et al., 2022a). It is critical to select the most appropriate AH input under different AH coupling schemes for various climate and urban canopy numerical models (Molnar et al., 2020; Narumi et al., 2009). Currently, the dominant coupling scheme in studies is to use the AH obtained through inventory-based methods as sensible heat, but latent and storage heat should not be disregarded as they are important energy dissipation pathways (Vahmani et al., 2022; Yu et al., 2021). Therefore, the scarcity of comparative simulation studies using multiple AH inputs hinders a thorough understanding of the urban thermal environment, thus limiting the development of AH-based UHI mitigation measures.

In contrast, despite extensive research into UHI driving mechanisms, it is difficult to propose feasible thermal environment mitigation measures for developed land, whereas AH is controllable as an important heat source within cities, and such control has been effective in UHI mitigation (Liu et al., 2022b). Therefore, future research should focus on a deeper analysis and simulation of AH to achieve a reduction in energy consumption and an increase in urban thermal comfort through the reasonable control of AH. However, the differences in AH effects on the urban thermal environment are heavily influenced by the background climate, resulting in some synchronization with UHII variations as well as notable regional differences. As a result of the spatial and temporal heterogeneity of UHI and driving mechanisms, thermal mitigation measures must be tailored to local and temporal conditions, particularly in regions where the background environment differs markedly from the general situation, as in the particular characteristics of Lanzhou and Guangzhou in this study. The continental arid climate, urban basin topography, and large amount of bare soil around urban areas contribute to the cold island effect during daytime in Lanzhou, whereas in Guangzhou, the warm and rainy climate results in dense and moist land around the urban area, implying higher thermal inertia (Hafner and Kidder, 1999; Pandey et al., 2014), which may be an important reason for the considerably nighttime UHI. Other regions have unique characteristics that contribute to the variability of

AH driving effects. However, the strong UHI and AH effects in the summer are an urgent concern. Even if the AH input cannot be reduced, its warming effect can be mitigated to some extent by adjusting other potential drivers, such as increasing urban vegetation cover and building material albedo, or altering the urban landscape structure. However, although the UHI is high at night in winter, this additional heat helps to improve thermal comfort in cold climates and reduces heating energy consumption, demonstrating how capitalizing on the warming impact of AH and ΔS works in cold scenarios. This study serves as an important theoretical foundation for analyzing UHI from the perspective of AH and provides new ideas for more precise urban climate simulations to serve as more effective urban thermal environment optimization measures.

5.3. Limitations and uncertainties

The underlying mechanism of urban heat islands is a complex integration of multiple factors (Hu et al., 2020), particularly in multi-regional and multi-temporal analyses, making it challenging to arrive at a uniform and systematic conclusion. Furthermore, this study considered the impact of AH using two models, producing some reasonable results overall, but it was difficult to gain a thorough understanding of the physical mechanism in all regions and at all times due to the limitation of the scale of this study (Peng et al., 2012). More rigorous analyses can be performed for specific regions and time phases. Furthermore, due to cumulative parametric errors in the equation residuals, RS-SEB may produce larger errors in non-urban areas with less precise parameter settings than in urban areas, and the uncertainty assumptions raise some issues (Park et al., 2016; Sailor, 2011). Therefore, improving the accuracy of the estimations of the SEB terms and their parameters is a priority for subsequent studies. Possible areas of improvement in the future could include more reasonable heat storage models, finer meteorological observation data, and high-resolution multispectral remote sensing images for improved AH estimations based on RS-SEB.

6. Conclusion

This study investigated the differences in the spatial and temporal distributions and impacts of different AH models and their relationships with UHI. First, we estimated AH using an RS-SEB model, an improved energy consumption-machine learning model, and nighttime ΔS in seven Chinese cities, extracted the UHI based on remote-sensing LST, and analyzed the driving effects of AH on UHI and the interactions with other factors using a linear mixed-effects model and geographic detectors.

Although AH_{inv} and AH_{seb} were similar in distribution, there were considerable differences in temporal and spatial details, with AH_{inv} showing more aggregation in urban centers and radiating outward, whereas AH_{seb} was relatively weaker. AH_{seb} was notably weaker than AH_{inv} during the daytime in winter. UHI was strong during summer daytime and winter nighttime and has a stronger positive relationship with AH_{inv} at this time, whereas AH_{seb} and ΔS had a stronger linear correlation with UHI than AH_{inv}. The mixed-effects model confirmed the inherent warming effect of AH on the cities, but also showed the significance of background climatic factors in affecting the differences between AH_{inv} and AH_{seb} and their relationship with UHI. According to the geographic detectors, AH_{inv} had a stronger impact on UHI during the daytime and nighttime in summer and winter than at other times, and the driving effects of AH_{seb} and ΔS were stronger. The interaction of other potential driving factors with AH enhanced the interpretation rate of UHI, and the general trend of the interaction effects was similar to that of separate AH effects, but varied considerably between different factors. The surface albedo had a more salient impact on the AH_{inv} driving effects, whereas the interaction of AH_{seb} with other factors had a high interpretation rate (close to 100%).

AH obtained based on different methods has different implications in various spatial and temporal scenarios, and it is necessary to clarify the definition of AH in urban thermal environment research to reach more scientific and rigorous conclusions. In addition, the selection of AH inputs that match the coupling scheme of numerical and urban canopy models is an important topic that cannot be ignored in future urban climate simulations. More crucially, AH is the most important controllable driving factor of UHI and the key to a feasible urban thermal comfort optimization scheme, although the situational heterogeneity in the role of AH requires attention.

Acknowledgement

This work was funded by the National Natural Science Foundation of China [grant numbers 42201384, 42171357]; the National Natural Science Foundation of China Major Program [grant numbers 42192580, 42192584].

Reference

Alhazmi, M., Sailor, D.J., Anand, J., 2022. A new perspective for understanding actual anthropogenic heat emissions from buildings. Energy Build. 258, 111860. https://doi.org/10.1016/j.enbuild.2022.111860

Bahi, H., Mastouri, H., Radoine, H., 2019. Review of methods for retrieving urban heat islands. 3rd International Conference on Materials and environmental Science (ICMES). 27, 3004-3009. https://doi.org/10.1016/j.matpr.2020.03.272

Bollen, K.A., Brand, J.E., 2010. A General Panel Model with Random and Fixed Effects A Structural Equations Approach. Soc. Forces 89, 1-34. https://doi.org/10.1353/sof.2010.0072

Cao, Q., Yu, D.Y., Georgescu, M., Wu, J.G., 2016. Impacts of urbanization on summer climate in China: An assessment with coupled land-atmospheric modeling. J. Geophys. Res.-Atmos. 121, 10505-10521. https://doi.org/10.1002/2016jd025210

Chapman, S., Watson, J.E.M., Salazar, A., Thatcher, M., McAlpine, C.A., 2017. The impact of urbanization and climate change on urban temperatures: a systematic review. Landscape Ecol. 32, 1921-1935. https://doi.org/10.1007/s10980-017-0561-4

Chen, F., Yang, X., Wu, J., 2016. Simulation of the urban climate in a Chinese megacity with spatially heterogeneous anthropogenic heat data. J. Geophys. Res.-Atmos. 121, 5193-5212. https://doi.org/10.1002/2015jd024642

Chen, Q., Yang, X., Ouyang, Z., Zhao, N., Jiang, Q., Ye, T., Qi, J., Yue, W., 2020. Estimation of anthropogenic heat emissions in China using Cubist with points-of-interest and multisource remote sensing data. Environ. Pollut. 266, 115183. https://doi.org/10.1016/j.envpol.2020.115183

Chow, W.T.L., Salamanca, F., Georgescu, M., Mahalov, A., Milne, J.M., Ruddell, B.L., 2014. A multi-method and multi-scale approach for estimating city-wide anthropogenic heat fluxes. Atmos. Environ. 99, 64-76. https://doi.org/10.1016/j.atmosenv.2014.09.053

Clinton, N., Gong, P., 2013. MODIS detected surface urban heat islands and sinks: Global locations and controls. Remote Sens. Environ. 134, 294-304. https://doi.org/10.1016/j.rse.2013.03.008

Cong, J.P., Wang, L.B., Liu, F.J., Qian, Z.M., McMillin, S.E., Vaughn, M.G., Song, Y.M., Wang, S.S., Chen, S.S., Xiong, S.M., Shen, X.B., Sun, X., Zhou, Y.Z., Ho, H.C., Dong, G.H., 2022. Associations between metabolic syndrome and anthropogenic heat emissions in northeastern China. Environ. Res. 204, 111974. https://doi.org/10.1016/j.envres.2021.111974

Dewan, A., Kiselev, G., Botje, D., Mahmud, G.I., Bhuian, M.H., Hassan, Q.K., 2021. Surface urban heat island intensity in five major cities of Bangladesh: Patterns, drivers and trends. Sust. Cities Soc. 71, 102926. https://doi.org/10.1016/j.scs.2021.102926

Dong, Y., Varquez, A.C.G., Kanda, M., 2017. Global anthropogenic heat flux database with high spatial resolution. Atmos. Environ. 150, 276-294. https://doi.org/10.1016/j.atmosenv.2016.11.040

Firozjaei, M.K., Weng, Q.H., Zhao, C.H., Kiavarz, M., Lu, L.L., Alavipanah, S.K., 2020. Surface anthropogenic heat islands in six megacities: An assessment based on a triplesource surface energy balance model. Remote Sens. Environ. 242, 111751. https://doi.org/10.1016/j.rse.2020.111751

Fu, X., Yao, L., Xu, W., Wang, Y., Sun, S., 2022. Exploring the multitemporal surface urban heat island effect and its driving relation in the Beijing-Tianjin-Hebei urban agglomeration. Appl. Geogr. 144, 102714. https://doi.org/10.1016/j.apgeog.2022.102714

Gao, S., Janowicz, K., Couclelis, H., 2017. Extracting urban functional regions from points of interest and human activities on location-based social networks. T. gis 21, 446-467. https://doi.org/10.1111/tgis.12289

Gong, P., Li, X., Wang, J., Bai, Y., Cheng, B., Hu, T., Liu, X., Xu, B., Yang, J., Zhang, W., Zhou, Y., 2020. Annual maps of global artificial impervious area (GAIA) between 1985 and 2018. Remote Sens. Environ. 236, 111510. https://doi.org/10.1016/j.rse.2019.111510

Gong, P., Liu, H., Zhang, M., Li, C., Wang, J., Huang, H., Clinton, N., Ji, L., Li, W., Bai, Y., Chen, B., Xu, B., Zhu, Z., Yuan, C., Suen, H.P., Guo, J., Xu, N., Li, W., Zhao, Y., Yang, J., Yu, C., Wang, X., Fu, H., Yu, L., Dronova, I., Hui, F., Cheng, X., Shi, X., Xiao, F., Liu, Q., Song, L., 2019. Stable classification with limited sample: transferring a 30-m resolution sample set collected in 2015 to mapping 10-m resolution global land cover in 2017. Sci. Bull. 64, 370-373. https://doi.org/10.1016/j.scib.2019.03.002

Gu, S.H., Huang, C.R., Bai, L., Chu, C., Liu, Q.Y., 2016. Heat-related illness in China, summer of 2013. Int. J. Biometeorol. 60, 131-137. https://doi.org/10.1007/s00484-015-1011-0

Hafner, J., Kidder, S.Q., 1999. Urban heat island modeling in conjunction with satellite-derived surface/soil parameters. J. Appl. Meteorol. 38, 448-465. https://doi.org/10.1175/1520-0450(1999)038<0448:Uhimic>2.0.Co;2

Hu, D., Meng, Q., Zhang, L., Zhang, Y., 2020. Spatial quantitative analysis of the potential driving factors of land surface temperature in different "Centers" of polycentric cities: A case study in Tianjin, China. Sci. Total Environ. 706, 135244. https://doi.org/10.1016/j.scitotenv.2019.135244

Hu, D., Meng, Q.Y., Schlink, U., Hertel, D., Liu, W.X., Zhao, M.F., Guo, F.X., 2022. How do urban morphological blocks shape spatial patterns of land surface temperature over different seasons? A multifactorial driving analysis of Beijing, China. Int. J. Appl. Earth Obs. Geoinf. 106, 102648. https://doi.org/10.1016/j.jag.2021.102648

Kato, S., Yamaguchi, Y., 2005. Analysis of urban heat-island effect using ASTER and ETM+ Data: Separation of anthropogenic heat discharge and natural heat radiation from sensible heat flux. Remote Sens. Environ. 99, 44-54. https://doi.org/10.1016/j.rse.2005.04.026

Kato, S., Yamaguchi, Y., 2007. Estimation of storage heat flux in an urban area using ASTER data. Remote Sens. Environ. 110, 1-17. https://doi.org/10.1016/j.rse.2007.02.011

Kotthaus, S., Grimmond, C.S.B., 2012. Identification of Micro-scale Anthropogenic CO2, heat and moisture sources - Processing eddy covariance fluxes for a dense urban environment. Atmos. Environ. 57, 301-316. https://doi.org/10.1016/j.atmosenv.2012.04.024

Liang, Z., Wu, S.Y., Wang, Y.Y., Wei, F.L., Huang, J., Shen, J.S., Li, S.C., 2020. The relationship between urban form and heat island intensity along the urban development gradients. Sci. Total Environ. 708, 135011. https://doi.org/10.1016/j.scitotenv.2019.135011

Liu, K., Li, X., Wang, S., Li, Y., 2020. Investigating the impacts of driving factors on urban heat islands in southern China from 2003 to 2015. J. Clean Prod. 254, 120141. https://doi.org/10.1016/j.jclepro.2020.120141

Liu, X., Yue, W.Z., Zhou, Y.Y., Liu, Y., Xiong, C.S., Li, Q., 2021. Estimating multi-temporal anthropogenic heat flux based on the top-down method and temporal downscaling methods in Beijing, China. Resour. Conserv. Recycl. 172, 105682. https://doi.org/10.1016/j.resconrec.2021.105682

Liu, Y., Luo, Z., Grimmond, S., 2022a. Revising the definition of anthropogenic heat flux from buildings: role of human activities and building storage heat flux. Atmos. Chem. Phys. 22, 4721-4735. https://doi.org/10.5194/acp-22-4721-2022

Liu, Z.H., Lai, J.M., Zhan, W.F., Bechtel, B., Voogt, J., Quan, J.L., Hu, L.Q., Fu, P., Huang, F., Li, L., Guo, Z., Li, J.F., 2022b. Urban Heat Islands Significantly Reduced by COVID-19 Lockdown. Geophys. Res. Lett. 49, e2021GL096842. https://doi.org/10.1029/2021gl096842

Meng, Q., Liu, W., Zhang, L., Allam, M., Bi, Y., Hu, X., Gao, J., Hu, D., Jancso, T., 2022. Relationships between Land Surface Temperatures and Neighboring Environment in Highly Urbanized Areas: Seasonal and Scale Effects Analyses of Beijing, China. Remote Sens. 14, 4340. https://doi.org/10.3390/rs14174340

Meng, Q., Zhang, L., Sun, Z., Meng, F., Wang, L., Sun, Y., 2018. Characterizing spatial and temporal trends of surface urban heat island effect in an urban main built-up area: A 12-year case study in Beijing, China. Remote Sens. Environ. 204, 826-837. https://doi.org/10.1016/j.rse.2017.09.019

Ming, Y.J., Liu, Y., Liu, X., 2022. Spatial pattern of anthropogenic heat flux in monocentric and polycentric cities: The case of Chengdu and Chongqing. Sust. Cities Soc. 78, 103628. https://doi.org/10.1016/j.scs.2021.103628

Mirzaei, P.A., Haghighat, F., 2010. Approaches to study Urban Heat Island - Abilities and limitations. Build. Environ. 45, 2192-2201. https://doi.org/10.1016/j.buildenv.2010.04.001

Mohajerani, A., Bakaric, J., Jeffrey-Bailey, T., 2017. The urban heat island effect, its causes, and mitigation, with reference to the thermal properties of asphalt concrete. J. Environ. Manage. 197, 522-538. https://doi.org/10.1016/j.jenvman.2017.03.095

Molnar, G., Kovacs, A., Gal, T., 2020. How does anthropogenic heating affect the thermal environment in a medium-sized Central European city? A case study in Szeged, Hungary. Urban CLim. 34, 100673. https://doi.org/10.1016/j.uclim.2020.100673

[dataset] Muñoz Sabater, J., 2019. ERA5-Land monthly averaged data from 1981 to present. https://doi.org/10.24381/cds.68d2bb3

Narumi, D., Kondo, A., Shimoda, Y., 2009. Effects of anthropogenic heat release upon the urban climate in a Japanese megacity. Environ. Res. 109, 421-431. https://doi.org/10.1016/j.envres.2009.02.013

[dataset] NCEI GIS Team, 2021. Hourly/Sub-Hourly Observational Data. V3.0.0. https://www.ncei.noaa.gov/maps/hourly/

Nie, W.-S., Sun, T., Ni, G.-H., 2014. Spatiotemporal characteristics of anthropogenic heat in an urban environment: A case study of Tsinghua Campus. Build. Environ. 82, 675-686. https://doi.org/10.1016/j.buildenv.2014.10.011

Pandey, A.K., Singh, S., Berwal, S., Kumar, D., Pandey, P., Prakash, A., Lodhi, N., Maithani, S., Jain, V.K., Kumar, K., 2014. Spatio - temporal variations of urban heat island over Delhi. Urban CLim. 10, 119-133. https://doi.org/10.1016/j.uclim.2014.10.005

Park, C., Schade, G.W., Werner, N.D., Sailor, D.J., Kim, C.-H., 2016. Comparative estimates of anthropogenic heat emission in relation to surface energy balance of a subtropical urban neighborhood. Atmos. Environ. 126, 182-191. https://doi.org/10.1016/j.atmosenv.2015.11.038

Peng, S.S., Piao, S.L., Ciais, P., Friedlingstein, P., Ottle, C., Breon, F.M., Nan, H.J., Zhou, L.M., Myneni, R.B., 2012. Surface Urban Heat Island Across 419 Global Big Cities. Environ. Sci. Technol. 46, 696-703. https://doi.org/10.1021/es2030438

Peng, T., Sun, C., Feng, S., Zhang, Y., Fan, F., 2021. Temporal and Spatial Variation of Anthropogenic Heat in the Central Urban Area: A Case Study of Guangzhou, China. ISPRS Int. Geo-Inf. 10, 160. https://doi.org/10.3390/ijgi10030160

Pigeon, G., Legain, D., Durand, P., Masson, V., 2007. Anthropogenic heat release in an old European agglomeration (Toulouse, France). Int. J. Climatol. 27, 1969-1981. https://doi.org/10.1002/joc.1530

Qian, J., Meng, Q., Zhang, L., Hu, D., Hu, X., Liu, W., 2022. Improved anthropogenic heat flux model for fine spatiotemporal information in Southeast China. Environ. Pollut. 299, 118917. https://doi.org/10.1016/j.envpol.2022.118917

Quah, A.K.L., Roth, M., 2012. Diurnal and weekly variation of anthropogenic heat emissions in a tropical city, Singapore. Atmos. Environ. 46, 92-103. https://doi.org/10.1016/j.atmosenv.2011.10.015

Raj, S., Paul, S.K., Chakraborty, A., Kuttippurath, J., 2020. Anthropogenic forcing exacerbating the urban heat islands in India. J. Environ. Manage. 257, 110006. https://doi.org/10.1016/j.jenvman.2019.110006

Ramirez-Aguilar, E.A., Lucas Souza, L.C., 2019. Urban form and population density: Influences on Urban Heat Island intensities in Bogota, Colombia. Urban CLim. 29, 100497. https://doi.org/10.1016/j.uclim.2019.100497

Rizwan, A.M., Dennis, Y.C.L., Liu, C.H., 2008. A review on the generation, determination and mitigation of Urban Heat Island. J. Environ. Sci. 20, 120-128. https://doi.org/10.1016/s1001-0742(08)60019-4

Rozenfeld, H.D., Rybski, D., Andrade Jr, J.S., Batty, M., Stanley, H.E., Makse, H.A., 2008. Laws of population growth. P. Natl. Acad. Sci. 105, 18702-18707. https://doi.org/10.1073/pnas.0807435105

Sailor, D.J., 2011. A review of methods for estimating anthropogenic heat and moisture emissions in the urban environment. Int. J. Climatol. 31, 189-199. https://doi.org/10.1002/joc.2106

Schneider, A., Mertes, C.M., 2014. Expansion and growth in Chinese cities, 1978-2010. Environ. Res. Lett. 9, 024008. https://doi.org/10.1088/1748-9326/9/2/024008

Sheiner, L.B., Grasela, T.H., 1991. An introduction to mixed effect modeling: concepts, definitions, and justification[J]. Journal of pharmacokinetics and biopharmaceutics. J. Pharmacokinet. Biop. 19, S11-S24. https://doi.org/10.1007/bf01371005

Singh, V.K., Mughal, M.O., Martilli, A., Acero, J.A., Ivanchev, J., Norford, L.K., 2022. Numerical analysis of the impact of anthropogenic emissions on the urban environment of Singapore. Sci. Total Environ. 806, 150534. https://doi.org/10.1016/j.scitotenv.2021.150534

Smith, C., Lindley, S., Levermore, G., 2009. Estimating spatial and temporal patterns of urban anthropogenic heat fluxes for UK cities: the case of Manchester. Theor. Appl. Climatol. 98, 19-35. https://doi.org/10.1007/s00704-008-0086-5

Sun, R., Wang, Y., Chen, L., 2018. A distributed model for quantifying temporal-spatial patterns of anthropogenic heat based on energy consumption. J. Clean Prod. 170, 601-609. https://doi.org/10.1016/j.jclepro.2017.09.153

Tadono, T., Nagai, H., Ishida, H., Oda, F., Naito, S., Minakawa, K., Iwamoto, H., 2016. GENERATION OF THE 30 M-MESH GLOBAL DIGITAL SURFACE MODEL BY ALOS PRISM. 23rd Congress of the International-Society-for-Photogrammetry-and-Remote-Sensing (ISPRS). 41, 157-162. https://doi.org/10.5194/isprsarchives-XLI-B4-157-2016

Tao, H.R., Xing, J., Pan, G.F., Pleim, J., Ran, L.M., Wang, S.X., Chang, X., Li, G.J., Chen, F., Li, J.H., 2022. Impact of anthropogenic heat emissions on meteorological parameters and air quality in Beijing using a high-resolution model simulation. Front. Environ. Sci. Eng. 16, 44. https://doi.org/10.1007/s11783-021-1478-3

Ulpiani, G., 2021. On the linkage between urban heat island and urban pollution island: Three-decade literature review towards a conceptual framework. Sci. Total Environ. 751, 141727. https://doi.org/10.1016/j.scitotenv.2020.141727

Vahmani, P., Luo, X., Jones, A., Hong, T., 2022. Anthropogenic heating of the urban environment: An investigation of feedback dynamics between urban micro-climate and decomposed anthropogenic heating from buildings. Build. Environ. 213, 108841. https://doi.org/10.1016/j.buildenv.2022.108841

Varquez, A.C.G., Kiyomoto, S., Khanh, D.N., Kanda, M., 2021. Global 1-km present and future hourly anthropogenic heat flux. Sci. Data 8, 1-14. https://doi.org/10.1038/s41597-021-00850-w

Voogt, J.A., Oke, T.R., 2003. Thermal remote sensing of urban climates. Remote Sens. Environ. 86, 370-384. https://doi.org/10.1016/s0034-4257(03)00079-8

Wang, J.-F., Hu, Y., 2012. Environmental health risk detection with GeogDetector. Environ. Modell. Softw. 33, 114-115. https://doi.org/10.1016/j.envsoft.2012.01.015

Wang, J.-F., Li, X.-H., Christakos, G., Liao, Y.-L., Zhang, T., Gu, X., Zheng, X.-Y., 2010. Geographical Detectors-Based Health Risk Assessment and its Application in the Neural Tube Defects Study of the Heshun Region, China. Int. J. Geogr. Inf. Sci. 24, 107-127. https://doi.org/10.1080/13658810802443457

Wang, K., Aktas, Y.D., Malki-Epshtein, L., Wu, D., Bin Abdullah, M.F.A., 2022a. Mapping the city scale anthropogenic heat emissions from buildings in Kuala Lumpur through a top-down and a bottom-up approach. Sust. Cities Soc. 76, 103443. https://doi.org/10.1016/j.scs.2021.103443

Wang, X.M., Meng, Q.Y., Zhang, L.L., Hu, D., 2021a. Evaluation of urban green space in terms of thermal environmental benefits using geographical detector analysis. Int. J. Appl. Earth Obs. Geoinf. 105, 102610. https://doi.org/10.1016/j.jag.2021.102610

Wang, Y., Yi, G., Zhou, X., Zhang, T., Bie, X., Li, J., Ji, B., 2021b. Spatial distribution and influencing factors on urban land surface temperature of twelve megacities in China from 2000 to 2017. Ecol. Indic. 125, 107533. https://doi.org/10.1016/j.ecolind.2021.107533

Wang, Y.C., Hu, D.Y., Yu, C., Di, Y.F., Wang, S.S., Liu, M.Q., 2022b. Appraising regional anthropogenic heat flux using high spatial resolution NTL and POI data: A case study in the Beijing-Tianjin-Hebei region, China. Environ. Pollut. 292, 118359. https://doi.org/10.1016/j.envpol.2021.118359

Wang, Z., Meng, Q., Allam, M., Hu, D., Zhang, L., Menenti, M., 2021c. Environmental and anthropogenic drivers of surface urban heat island intensity: A case-study in the Yangtze River Delta, China. Ecol. Indic. 128, 107845. https://doi.org/10.1016/j.ecolind.2021.107845

Ward, K., Lauf, S., Kleinschmit, B., Endlicher, W., 2016. Heat waves and urban heat islands in Europe: A review of relevant drivers. Sci. Total Environ. 569, 527-539. https://doi.org/10.1016/j.scitotenv.2016.06.119

Wolpert, D.H., 1992. Stacked generalization. Neural Networks 5, 241-259. https://doi.org/https://doi.org/10.1016/S0893-6080(05)80023-1

Wong, M.S., Yang, J.X., Nichol, J., Weng, Q.H., Menenti, M., Chan, P.W., 2015. Modeling of Anthropogenic Heat Flux Using HJ-1B Chinese Small Satellite Image: A Study of Heterogeneous Urbanized Areas in Hong Kong. IEEE Geosci. Remote Sens. Lett. 12, 1466-1470. https://doi.org/10.1109/lgrs.2015.2409111

Wu, Y., Hou, H., Wang, R., Murayama, Y., Wang, L., Hu, T., 2022. Effects of landscape patterns on the morphological evolution of surface urban heat island in Hangzhou during 2000-2020. Sust. Cities Soc. 79, 103717. https://doi.org/10.1016/j.scs.2022.103717

Xu, D., Zhou, D., Wang, Y.P., Meng, X.Z., Gu, Z.L., Yang, Y.J., 2021. Temporal and spatial heterogeneity research of urban anthropogenic heat emissions based on multi-source spatial big data fusion for Xi'an, China. Energy Build. 240, 110884. https://doi.org/10.1016/j.enbuild.2021.110884

Yang, B., Liu, H., Kang, E.L., Hawthorne, T.L., Tong, S.T.Y., Shu, S., Xu, M., 2022a. Traffic restrictions during the 2008 Olympic Games reduced urban heat intensity and extent in Beijing. Commun. Earth Environ. 3, 105. https://doi.org/10.1038/s43247-022-00427-4

Yang, B., Yang, X., Leung, L.R., Zhong, S., Qian, Y., Zhao, C., Chen, F., Zhang, Y., Qi, J., 2019. Modeling the Impacts of Urbanization on Summer Thermal Comfort: The Role of Urban Land Use and Anthropogenic Heat. J. Geophys. Res.-Atmos. 124, 6681-6697. https://doi.org/10.1029/2018jd029829

Yang, M., Wang, H., Yu, C.W., Cao, S.-J., 2022b. A global challenge of accurately predicting building energy consumption under urban heat island effect. Indoor Built Environ., 1420326x221123222. https://doi.org/10.1177/1420326x221123222

Yang, Q., Huang, X., Li, J., 2017. Assessing the relationship between surface urban heat islands and landscape patterns across climatic zones in China. Sci. Rep. 7, 9337.

https://doi.org/10.1038/s41598-017-09628-w
Yu, Z., Hu, L.Q., Sun, T., Albertson, J., Li, Q., 2021. Impact of heat storage on remote-sensing based quantification of anthropogenic heat in urban environments. Remote Sens. Environ. 262, 112520. https://doi.org/10.1016/j.rse.2021.112520
Zhan, C., Xie, M., 2022. Land use and anthropogenic heat modulate ozone by meteorology: a perspective from the Yangtze River Delta region. Atmos. Chem. Phys. 22, 1351-1371. https://doi.org/10.5194/acp-22-1351-2022
Zhao, G.S., Liu, J.Y., Kuang, W.H., Ouyang, Z.Y., Xie, Z.L., 2015. Disturbance impacts of land use change on biodiversity conservation priority areas across China: 1990-2010. J. Geogr. Sci. 25, 515-529. https://doi.org/10.1007/s11442-015-1184-9
Zhao, L., Lee, X., Smith, R.B., Oleson, K., 2014. Strong contributions of local background climate to urban heat islands. Nature 511, 216-219. https://doi.org/10.1038/nature13462
Zheng, Y., Huang, L., Zhai, J., 2021. Divergent trends of urban thermal environmental characteristics in China. J. Clean Prod. 287, 125053. https://doi.org/10.1016/j.jclepro.2020.125053
Zheng, Y., Weng, Q., 2018. High spatial- and temporal-resolution anthropogenic heat discharge estimation in Los Angeles County, California. J. Environ. Manage. 206, 1274-1286. https://doi.org/10.1016/j.jenvman.2017.07.047
Zhou, D.C., Zhao, S.Q., Liu, S.G., Zhang, L.X., Zhu, C., 2014. Surface urban heat island in China's 32 major cities: Spatial patterns and drivers. Remote Sens. Environ. 152, 51-61. https://doi.org/10.1016/j.rse.2014.05.017
Zhou, Y., Weng, Q., Gurney, K.R., Shuai, Y., Hu, X., 2012. Estimation of the relationship between remotely sensed anthropogenic heat discharge and building energy use. ISPRS-J. Photogramm. Remote Sens. 67, 65-72. https://doi.org/10.1016/j.isprsjprs.2011.10.007
Zhou, Y.Y., Li, X.C., Asrar, G.R., Smith, S.J., Imhoff, M., 2018. A global record of annual urban dynamics (1992-2013) from nighttime lights. Remote Sens. Environ. 219, 206-220. https://doi.org/10.1016/j.rse.2018.10.015